ACS APPLIED ENERGY MATERIALS

www.acsaem.org

Forum Article

Fabrication of Single Metal−Organic Framework Crystal Devices to Inform Energy Conversion Platforms

Dara E. Weiss, Yifei Zhu, Kathryn Kingsbury, Nicholas Blumenschein, Adam L. Friedman, Aubrey T. Hanbicki, and Thomas J. Kempa*

Cite This: https://doi.org/10.1021/acsaem.3c02456

Read Online

ACCESS | Metrics & More | Article Recommendations | Supporting Information

ABSTRACT: Stimulus-responsive metal−organic frameworks (MOFs) are compelling candidates for the active components of sensors, actuators, low-power electronics, and energy conversion platforms. However, strategies to precisely integrate single MOF crystals into devices, a crucial condition for fully exploiting their potential in high-performance and energy applications, are lacking. Here, we provide a primer on best practices in the fabrication of high quality devices from single MOF crystals. We discuss how to synthesize and configure MOFs for integration into devices, identify optimal lithography conditions, and define contacts to and measure devices to extract the maximum insight into the transport physics of these materials. Using a MOF composed of Mo_2(isonicotinate)$_4$ clusters as an exemplar, we apply these fabrication protocols to prepare two-terminal and three-terminal field-effect transistor devices. Measurements of these devices reveal the MOF to have a conductivity of ∼1 mS cm^{-1}, a *p*-type behavior, and an underlying conductance anisotropy, all of which directly reflect the mixed valency and unique topology of the MOF. Our efforts seek to provide a more efficient route toward fabricating MOF-based devices and, by so doing, aim to advance the community's understanding of transport physics in MOFs and to inform how best to integrate them into next-generation energy conversion and storage platforms.

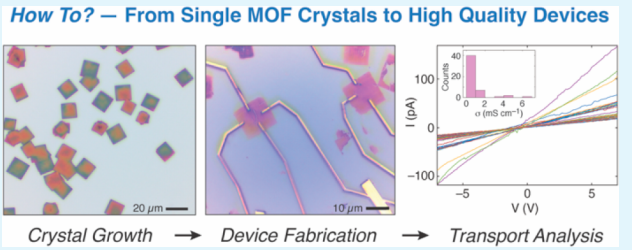

KEYWORDS: *metal−organic frameworks, energy, devices, fabrication, transistors, single crystals*

INTRODUCTION

While metal−organic frameworks (MOFs) have a well-established use case in applications involving storage,[1,2] separations,[1−3] and catalysis,[1,3−5] recent attention has focused on exploiting their inherently tunable structure and electronic transport properties in devices for integrated energy conversion,[6] sensing,[7,8] and memory.[9−11] Indeed, successful implementation of MOFs as the *active* components of energy storage and conversion platforms (e.g., for controlling photoinduced or electron-induced reactions) relies on a detailed understanding of charge transport, which can be reliably gleaned from electronic studies of high quality devices. Two critical challenges must be addressed to realize MOF-based active electronic devices: (1) synthesis of high quality crystalline MOFs in the desired form (2D monolayer, thin film, bulk crystal powder) for incorporation into devices and (2) fabrication and measurement of devices to extract reliable information on the intrinsic electronic transport properties of the MOF. This article focuses on the latter challenge and seeks to provide best practices for fabricating high-quality devices to single MOF crystals. By focusing attention on key protocols and considerations in device fabrication, many of which may not be familiar to researchers in the MOF community, we hope to advance studies of electronic transport phenomena in these intriguing molecular materials and, by extension, to accelerate their adoption within emerging energy conversion platforms.

For purposes of the discussion herein, devices will be fabricated on ultrathin (<100 nm thick) single crystals composed of layered 2D MOFs,[12−15] but many of the best practices (lithography conditions, metal contacts, solvent processing conditions, etc.)[16] apply well to MOFs having different compositions, sizes, and dimensionalities. For devices composed of very large MOF crystals (e.g., those with dimensions approaching mm), we turn the reader's attention to the many excellent reviews on the application of macroscale fabrication processes. It is important to reinforce the choice to prepare and measure devices at the single crystal limit. This is done in order to identify as much as possible the "true" intrinsic charge transport processes of the MOF by isolating extrinsic factors such as intergrain hopping, shunting, or charge leakage through conductive additives (e.g., ionic liquids) or

Special Issue: Metal-Organic Frameworks for Energy Storage Applications

Received: September 28, 2023
Revised: November 15, 2023
Accepted: November 21, 2023

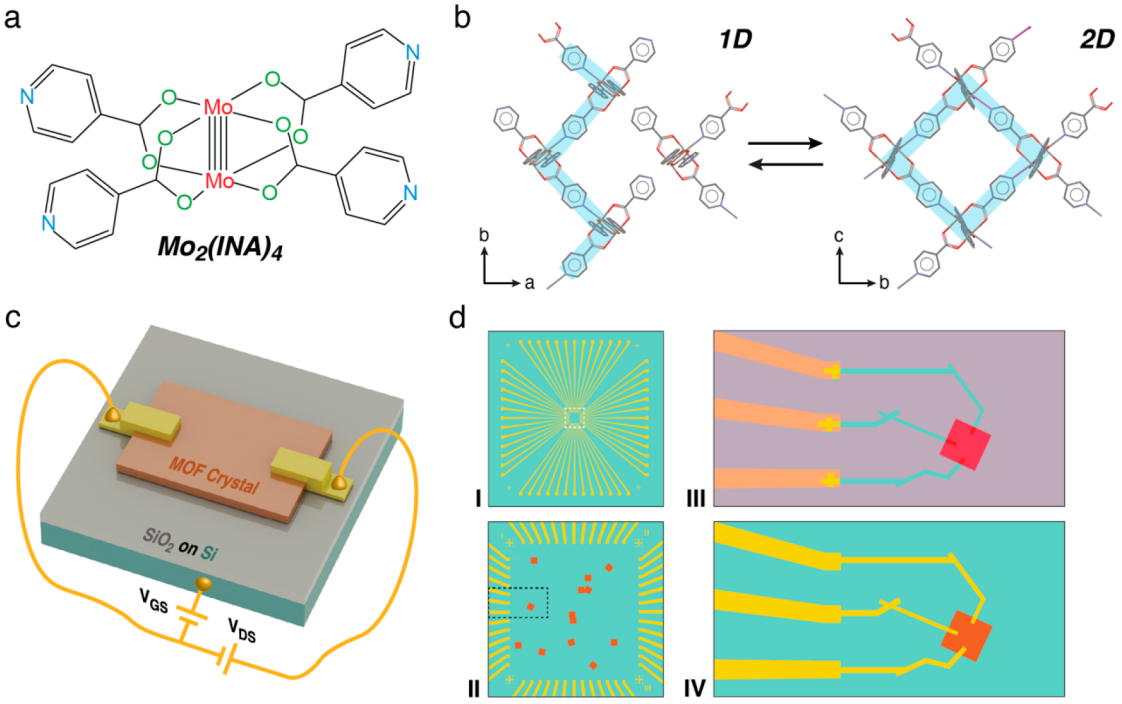

Figure 1. (a) Chemical structure of a Mo_2(isonicotinate)$_4$ paddlewheel cluster. (b) Single crystal structure of a CVD grown MOF composed of Mo_2(isonicotinate)$_4$ clusters. The 1D zigzag chains are highlighted. At the right is the crystal structure of the MOF when it assumes a 2D topology following exposure to dimethylacetamide. (c) Schematic of a MOF-based field-effect transistor. In this architecture, the channel is composed of the MOF. (d) Outline of the principal device fabrication steps: First, a (I) plasma cleaned substrate (SiO_2 in this example) is photolithographically patterned with outer electrodes and fiducial markers. Second, (II) single MOF crystals (Mo_2(isonicotinate)$_4$ in this example) are grown from the gas phase onto the fiducially marked substrate. Next, (III) resist is deposited over the MOF crystals and substrate, and electron-beam lithography is used to pattern what will become the electrodes over each individual MOF crystal. Finally, (IV) metal contacts (e.g., Ti/Au) are deposited, and a resist lift-off step concludes the device fabrication.

trapping at interfaces and impurities. Many of these extrinsic factors can contribute significantly to the reported performance of some MOF devices, thus complicating the rigorous interpretation of transport data. By excluding these contributions, we can provide a deeper assessment of electronic transport mechanisms and a clearer understanding of how to preserve intrinsic MOF performance at the scale of large devices.

Measurements of single MOF crystal devices not only fulfill a vital spectroscopic need in identifying principal carrier transport mechanisms, but also provide a convenient means to produce high-performance prototypes to assess the promise of a MOF for a given application.[2,12−14,17,18] For example, with the advent of new 2D MOFs and 2D covalent organic frameworks (COFs),[12−14,19−22] there is the opportunity to use devices to trace the evolution of electronic transport within these porous frameworks as a function of their topology, chemical composition, and dimensionality.[38−40] Moreover, single-crystal device measurements can help identify fundamental performance limits (e.g., related to field-effect response, optical response, chemical response, phase change) that can directly inform the design of full-scale technology prototypes.

Despite these opportunities, reliable protocols for the fabrication of single MOF crystal devices are lacking. In this contribution, we demonstrate that high quality field-effect transistors (FETs)[23] can be fabricated from single ultrathin 2D MOF crystals. The FETs exhibit *p*-type channel characteristics reflective of hole-mediated transport through the MOF crystals, which are composed of 2D sheets assembled from Mo_2(isonicotinate)$_4$ clusters.[12−14] We share the principal design considerations with regard to gas-phase growth optimization, lithography, and deposition of contact metals after patterning by lithography that yield such high quality devices. Through this contribution, we aim to fill the knowledge gaps regarding methods for reliable and generalizable single MOF crystal device fabrication.

RESULTS AND DISCUSSION

Synthesis of Ultrathin MOF Crystals by Chemical Vapor Deposition. Gas-phase growth of single ultrathin MOF crystals directly onto substrates suitable for device fabrication offers several advantages. First, direct growth obviates the often laborious process of exfoliating and transferring bulk materials or polycrystalline films from growth substrates to the substrates on which the devices will be fabricated. Such postsynthetic manipulation can sometimes damage the crystals, prevent them from properly adhering to or interacting with the substrate, and introduce residue that interferes with the MOF or the contact quality. Second, gas-phase synthesis affords the opportunity to tune between the extremes of self-limited monolayer MOF crystal growth and predominantly out-of-plane growth, which yields bulk crystals. Finally, gas-phase growth is compatible with established industrial methods for processing electronic and optical devices and, in particular, has the added benefit of avoiding the use of solvents, which could contaminate key surfaces and interfaces during the process of monolithic device integration.[1,15,17,24−27] Monolithic integration, which refers to the incorporation of many discrete circuit components onto a single substrate,

https://doi.org/10.1021/acsaem.3c02456
ACS Appl. Energy Mater. XXXX, XXX, XXX−XXX

Table 1. Optimized Parameters and Fabrication Considerations

Parameter	Optimal Condition	Rationale
Crystal Thickness	20−800 nm	Avoid overly thick crystals that may impede lift off and become damaged in the process.
Crystal Area	100−400 μm^2	Provide sufficient edge length to accommodate multiple contacts and configurations.
Metal Choice	Ti/Cr: adhesion layer; Au: contact layer	Ti and Cr help to adhere and stabilize the Au contact layer to the device substrate. In this case, Au makes an ohmic contact to the MOF.
E-beam Lithography	Probe current: 1 nA; Dose: 1500 $\mu C/cm^2$; Acc. Voltage: 100 kV; Pitch: 5 nm	Conditions will vary based on knock-on damage thresholds for a given MOF. These conditions provide for sufficient resolution and resist exposure while minimizing e-beam induced crystal damage.
Resist Development	Stir 60 s in a 1:3 MIBK:IPA mixture; rinse 30 s in IPA; dry under N_2 stream	A relatively short development time is sufficient to ensure high pattern fidelity. The 30 s isopropanol rinse cleans the substrate of any residue.
Thermal Evaporator	Pressure: 3.8×10^{-7} mbar; Dep. rate: 0.5 Å/s (Ti/Cr) 1−2 Å/s (Au)	Pressures below 1×10^{-6} mbar ensure stable evaporation of metal, especially Ti which is prone to gettering residual O_2 from the chamber. Slow deposition rates ensure good adhesion and mechanically stable metal films.
Lift Off	45 min in acetone followed immediately by gentle IPA rinse and drying under gentle N_2 stream	Acetone reliably removes PMMA/MMA resist layers without harming the MOF crystals. Isopropanol evaporates more slowly, ensuring crystals are not sheared from the substrate.

provides a convenient and efficient opportunity for scalable chip production.

We previously reported the gas-phase growth by chemical vapor deposition (CVD) of single-crystal MOFs composed of Mo_2(isonicotinate)$_4$ paddlewheel clusters.[12−14] The devices reported herein will utilize this chemically and electrically responsive 2D MOF. These paddlewheel clusters exhibit redox-active and mixed-valence[28−30] characteristics that facilitate charge transport through the MOF lattice (Figure 1a). Moreover, the solvent tunable coordination of the pyridinyl N to the axial positions of the Mo_2 core can be used to reversibly switch the framework between a 1D partially coordinated phase and a 2D fully coordinated MOF phase (Figure 1b).[13] Two-terminal and three-terminal field-effect transistor (FET) devices will allow us to determine the conductance, saturation response, in which the device carries a constant current above a certain value of the applied gate voltage, majority carrier (ie., electron or hole) type and mobility, and any other transport anomalies within the MOF (Figure 1c).[5,17,23,26]

While the fabrication of a MOF-based device follows the canonical steps of patterning, deposition, and lift off to define precisely ohmic metal contacts to a single MOF crystal (Figure 1d), there are many specific considerations that are discussed below and summarized in Table 1.

The first consideration when fabricating MOF devices is the provision of uniform MOF crystals of a desired thickness and a suitably large area. Crystals should typically cover areas of at least 20 μm^2 (ideally $\geq$100 μm^2) so that multiple contacts and contact configurations can be patterned to the crystal (Figure 2a). This is done in order to accommodate, for example, four-point probe measurements that correct for contact resistance, Hall bar architectures for magnetoresistance and carrier mobility measurements, or contact configurations that sample direction-dependent current transport. The crystal thickness also critically influences the choice of the metal contact and resist layer thickness. In general, it is best for the crystals to be less than ~500 nm thick such that the contact metal stability and lift-off process are not compromised. For the contact to traverse over the crystal without excess strain or fracture, it is preferable for the metal layer to be at least as thick as the crystal. In turn, for proper lift off, the resist undercut layer(s)—in this case provided by methyl-methacrylate (MMA) copolymer—should be thicker (~2 ×) than the contact metal layer (Figure 2b). It is also important for the resist to be able to wet and deposit onto the crystal uniformly so that there are no thickness anomalies that would interfere with clean removal of residual resist and metal; this process is referred to as lift off. For these reasons, and with additional provisions to protect our crystals, for a device substrate containing our $\leq$150 nm thick MOF crystals, we used a 300 nm thick contact layer, a 1.5 μm thick MMA layer, and a 180 nm thick PMMA layer.

CVD can be used to grow single MOF crystals with the aforementioned device-suitable sizes and morphologies. While a full discussion of the CVD synthesis conditions is beyond the scope of this paper and indeed the conditions mentioned herein must be recognized as tailored for the synthesis of the 2D Mo_2(isonicotinate)$_4$ MOF, we summarize the key parameters controlling the crystal nucleation density, morphology, and uniformity. We perform MOF crystal growth within our CVD reactor at a pressure of 5 Torr and temperature of 315 °C (Supporting Information, Methods). Under these conditions, the modular paddlewheel cluster sublimes and then is swept into the cooler zone of our multizone CVD system whereupon it deposits and assembles into the MOF. Heating the solid Mo_2(isonicotinate)$_4$ precursor within the CVD reactor from room temperature to the synthesis hold temperature of 315 °C at rates of 19 °C/min reliably yields uniformly thin crystals. Optical images of the SiO_2 substrate reveal a high density (~1000 crystals per 1 mm^2) of well-dispersed and flat crystals (Figure 2c, Figure S1). Previously

https://doi.org/10.1021/acsaem.3c02456
ACS Appl. Energy Mater. XXXX, XXX, XXX−XXX

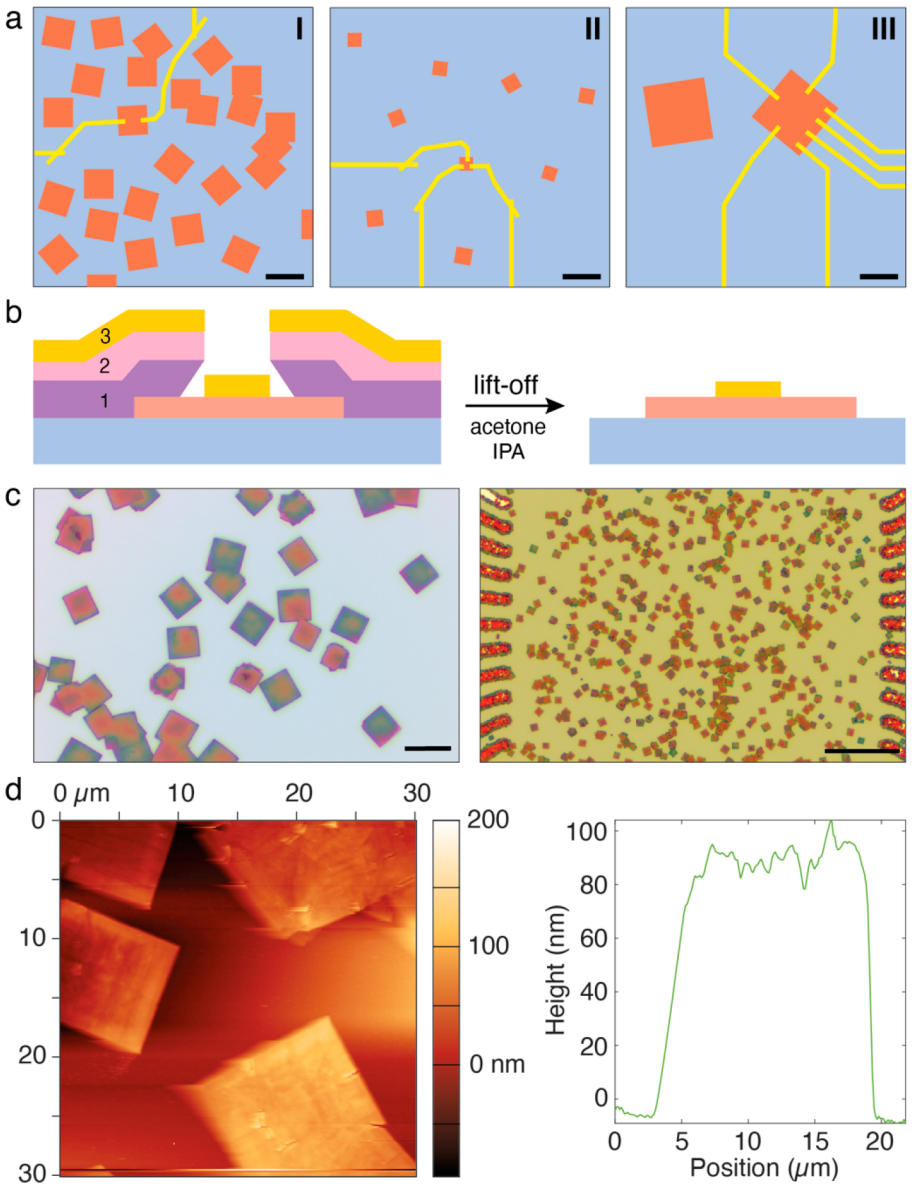

Figure 2. (a) Schematics showing a substrate with (I) an excessively high density of MOF crystals, (II) insufficiently large MOF crystals, and (III) a well-isolated large single MOF crystal, which is the ideal. (b) A schematic demonstrating the metal lift-off process in the presence of sufficient undercut. This condition is satisfied when 1 is thicker than 3, where 1 is the MMA layer, 2 is the PMMA layer, and 3 is the Au contact layer. (c) Optical images of MOF crystals before device fabrication, demonstrating ideal edge length, thickness, and dispersity on the growth substrate. Scale bars: 20 μm (left), 100 μm (right). (d) AFM map and corresponding line scan profile of a single MOF crystal.

published X-ray diffraction data[13] have identified these deposits as single crystals composed of 1D zig-zagging chains of the Mo_2(isonicotinate)$_4$ cluster. Henceforth, we refer to crystals of this 1D phase as product A. Atomic force microscopy (AFM) data reveal the crystals to be on average 61 nm thick with smooth (002) top surface planes and to be absent of crystal intergrowths or multiple twins (Figure 2d). We propose that the high precursor heating rate leads to abrupt nucleation that favors lateral growth over out-of-plane growth thus giving rise to thinner and flat crystals.

The nature of the substrate upon which the crystals are deposited must also be carefully considered, with respect to their growth and eventual incorporation into devices. First, the interaction of the substrate with the precursors of the MOF (in this case the Mo_2(isonicotinate)$_4$ clusters) dictates their in-plane diffusivity, and therefore, the degree to which self-limited in-plane growth of ultrathin to monolayer crystals can be expected. For example, using identical CVD conditions, we observe clear differences in the size, shape, and quality of crystals when grown on silicon with native oxide, HF-etched silicon, and mica substrates (Figure S2). Second, the use of substrates with insulating layers atop doped or conductive layers enables monolithic integration of the deposited crystals into an FET with a back-gate geometry. For the devices reported herein, we grow MOF crystals directly onto degenerately doped Si(100) substrates with a top layer of 200 nm thick SiO_2, which serves as an appropriate gate dielectric.[31,32] Finally, to facilitate identification of the crystals and design of the contact patterns for eventual electron-beam lithography (EBL), fiducial and alignment markers must be deposited on the substrate, ideally before crystal deposition. Such fiducial markers can typically be patterned photolitho-

https://doi.org/10.1021/acsaem.3c02456
ACS Appl. Energy Mater. XXXX, XXX, XXX−XXX

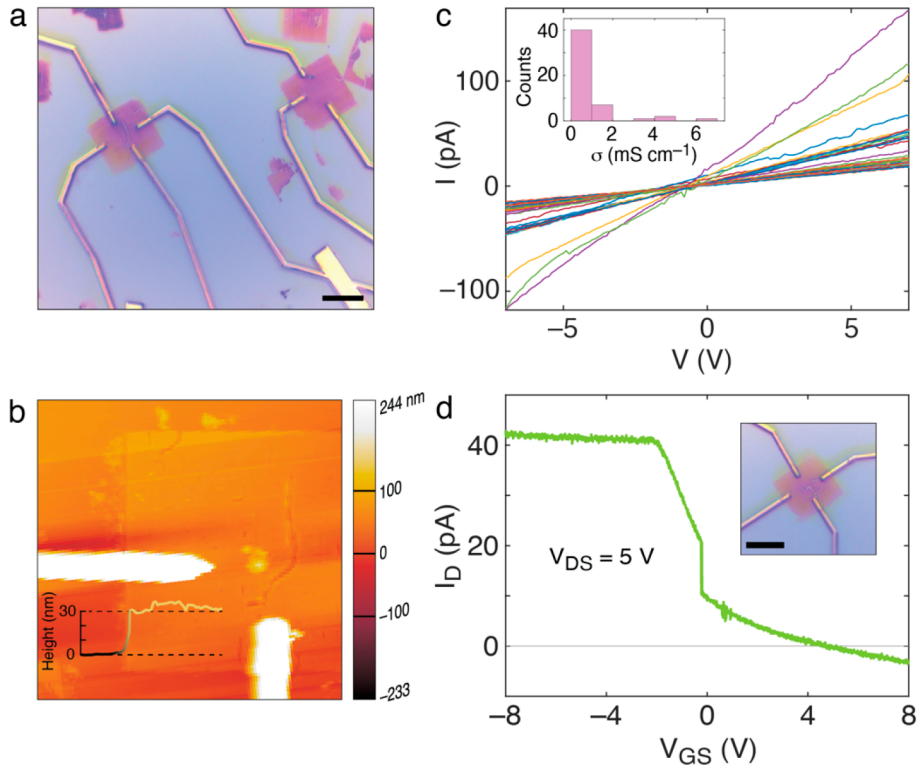

Figure 3. (a) Optical image of two single MOF crystal devices with multiple contact configurations. Scale bar: 10 μm. (b) AFM map of a two-contact device. (c) I_D−V_{SD} transfer characteristics for 51 devices. Current was recorded for each device across the voltage range shown in 10 mV increments. Inset: Distribution of calculated conductivity values from all 51 devices. (d) I_D−V_{GS} transfer characteristic (V_{DS} = +5 V) for a back-gated single MOF crystal device. Inset: Optical image of the device. Scale bar: 10 μm.

graphically and must be very accurately positioned and designed to reduce EBL pattern artifacts, such as misalignment, stretching, and biasing (Supporting Information, Methods). The fiducial marker should be composed of a thin layer of a metal (50 nm Au in the present case), which appears with a high contrast when imaged through optical and electron microscopes. Together, the aforementioned considerations ensure that the MOF crystals are appropriately sized and configured for device fabrication.

Fabrication of Single MOF Crystal Devices. Electron beam lithography (EBL) enables high-resolution patterning of contacts for micro- and nanoscale electronic devices but presents several challenges when applied to MOFs.[2,13,15,25] Briefly, in EBL a focused electron beam is rastered across a surface coated with a resist, usually a polymer such as poly(methyl methacrylate) (PMMA), to define a pattern. The polymeric chains in the resist undergo scission wherever they are exposed to the beam, and subsequent exposure to a solvent (in this case methyl-isobutylketone) removes the exposed areas, while leaving the unexposed areas untouched, to reveal a pattern. Metals are then deposited onto the entire substrate, whereupon they settle into the patterned relief and make physical contact with the exposed areas of the pattern. A thin (few Å) layer of metal, such as chromium or titanium, is typically deposited before the contact metal in order to enhance the adhesion (e.g., through mitigation of mechanical strain) of the contact metal to the substrate. The final step of fabrication involves lift off of the contact metals covering the remainder of the substrate to reveal metal contacts to the individual MOF crystals.

We optimized each step of our fabrication process to ensure the proper patterning and adhesion of the metal contacts while protecting the MOF crystals. A primary concern when working with organic species, especially porous coordination polymers, is electron beam-induced damage through knock-on effects (atomic displacement caused by incident electrons), radical cascades, and Joule heating, in which energy from the electron beam is converted to heat.[33−35] After testing many EBL conditions, we found that a 100 kV beam acceleration voltage, 1500 μC/cm^2 dose, and 1 nA total beam current were effective at patterning high-resolution features while mitigating any crystal damage (Figures S3, S4). Some MOFs may exhibit higher beam sensitivities, and thus, careful monitoring for beam damage and subsequent optimizations of the EBL conditions are crucial. Nevertheless, our conditions (Supporting Information, Methods) should serve as a promising starting point. The width and density of the patterned contacts also play a key role in defining the level of e-beam exposure the crystals are subjected to. For example, in our case, while 4 μm wide electrodes were patterned to overlap with the photolithographically defined global electrodes, their width was reduced to 0.5−1.5 μm at the point where they overlap the MOF crystals. Reducing the time that the e-beam dwells in the vicinity of the crystal reduces the total heating and charging (e.g., through secondary electron bombardment) that the crystal may experience, thereby mitigating damage. Of course, considerations taken to protect the crystal must be balanced against the need to properly expose the resist and to define contacts that are sufficiently robust to survive lift off.

The second consideration is the type and amount of electron-beam resist applied. As mentioned above, ample resist

https://doi.org/10.1021/acsaem.3c02456
ACS Appl. Energy Mater. XXXX, XXX, XXX−XXX

undercut (provided by layer(s) of MMA) ensures that there is a discontinuity in the metal contact layer between the material to which it is meant to be adhered and the top of the resist surface. This ensures clean and efficient metal lift off, and in order to accomplish this, we recommend that the undercut be at least as thick as the thickness of the contact metal layer(s). For crystals under 500 nm thick these procedures readily apply and produce high yields of good quality devices (Figure S5). However, the preparation of devices from crystals thicker than 1 μm requires additional attention. Several layers of MMA are required to fully wet and coat the crystal with resist such that the metal contact layer does not form a continuous point of contact with the top of the crystal, leading to device shorts or even physical lift off of the entire crystal. On the other hand, such additional layers of resist necessitate the use of higher beam currents and/or dwell times that increase the likelihood for resist bloating or crystal damage. In general, we recommend not exceeding contact metal thicknesses of 1 μm, if possible, so as to avoid potential issues with lift off and associated contact breakage (Figures S6, S7).

Finally, one must optimize the development and lift-off conditions to maintain the device integrity (Table 1). We recommend testing MOF crystals against a number of developer solvents for a range of candidate resists. Prior to selecting PMMA as the e-beam resist for our devices, we found that the ketone solvent developer does not degrade our 2D Mo_2(isonicotinate)$_4$ MOF crystals. Following pattern development, metal contacts (5 nm Ti followed by 300 nm Au) were deposited through thermal evaporation from a high vacuum (4×10^{-7} mbar). Evaporator chamber pressures $<1 \times 10^{-6}$ mbar are important to ensure steady metal evaporation, especially when evaporating Ti as this metal has a tendency to getter residual oxygen,[36] which can compromise the mechanical stability and conductivity of the metal contact layer (Figure S8). After metal deposition, lift off was performed by placing the substrate in a Petri dish with acetone for 45 min and then into isopropanol for rinsing, and finally the substrate was dried under a gentle stream of nitrogen. We caution allowing the lift-off solvent, especially one with a high vapor pressure, to evaporate from the substrate since rapid drying can generate strong capillary forces that may shear MOF crystals from the substrate (Figure S9). The sequential use of acetone followed by isopropanol moderates the drying process, thereby allowing for the gradual release of resist from the crystals.

Electronic Transport Data. Applying the fabrication protocols above to our model Mo_2(isonicotinate)$_4$ MOF yielded 51 devices on a single chip, with this number limited entirely by the number of available electrodes to which a single device configuration can be addressed. Out of 52 devices designed, 51 subsequently registered a clear electrical response for a high yield of 98%. Devices were fabricated to single MOF crystals in order to acquire three distinct transfer characteristics: (1) drain current versus source-drain voltage (I_D–V_{SD}) characteristics for parallel oriented contacts, (2) I_D–V_{SD} characteristics for perpendicular oriented contacts, and (3) drain current versus gate-source voltage (I_D–V_{GS}) characteristics (Figure 3a). Device channel lengths and cross-sectional areas were measured by AFM (Figure 3b). Conductivity values for each of the 51 device configurations were calculated using resistance values obtained from linear fits to the device I_D–V_{SD} data and the aforementioned measured geometries of the device channel (Figure 3c). Whereas the mean conductivity of devices with a perpendicular contact configuration is 1.12×10^{-5} S cm^{-1}, the mean conductivity of devices with a parallel contact configuration is 100 times greater at 1.80×10^{-3} S cm^{-1} (Figure 3c). The orientation of the crystals suggests that the parallel contact configuration should be commensurate with the 1D zigzag chain axis (Figure S10). We propose that the substantially higher conductivity for the parallel contact configurations reflects the apparent preference for charge injection and transport into and along the 1D chain. These results also underscore the importance of fabricating devices to single crystals because such studies better enable discovery of charge transport anomalies and more unambiguous determination of their molecular mechanisms.

Field-effect transistor transfer characteristics (I_D–V_{GS} data) were obtained on all of the aforementioned devices to gain insight into the underlying properties of the MOF channel. A single MOF crystal device subject to a V_{GS} sweep from −10 V to +10 V (at V_{DS} = +5 V) reveals an increasing conductance for negative values of V_{GS} with apparent saturation of I_D and modest on–off ratios (Figure 3d). These data indicate that the MOF channel is *p*-type. Indeed, previously published electron paramagnetic resonance (EPR) data collected on Mo_2(isonicotinate)$_4$ coordination polymers composed of 1D linear chains, which are analogous to the 1D zigzag architecture of the MOFs discussed herein, are consistent with the presence of Mo_2^V centers.[14,37] These prior results suggest that our MOF should be hole-doped and thereby corroborate our finding that the MOF channel shows *p*-type conductance under gate bias. Once again, these data reinforce how high-quality devices fabricated to single MOF crystals can be used to unambiguously identify the underlying charge transport physics in these materials.

CONCLUSIONS

We have described a set of reliable and generally applicable protocols and considerations for the fabrication of devices from single metal–organic framework crystals. To guide the community's future efforts in building and acquiring data from MOF devices, we have provided a comprehensive discussion of how MOF crystals should ideally be configured for integration into devices, how resist stacks should be chosen, how electron-beam dosages should be optimized, and what are the key considerations for metal deposition and lift off. Using these principles, we fabricated an exceptionally high yield of field-effect transistor devices from ultrathin crystals composed of Mo_2(isonicotinate)$_4$, a modular building unit for MOFs that exhibits mixed valency, redox activity, and reversible phase-change behavior. These devices revealed the MOF to be modestly conductive (~1 mS cm^{-1}) with *p*-type channel behavior and anisotropic conductance that reflects the MOF's underlying 1D zigzag chain topology. We intend this study not only as a primer on key methods and principles for fabrication of devices from single MOF crystals, but also as a reminder that such devices are vital for a deeper and more consolidated understanding of transport physics in MOFs. The accumulation of such fundamental knowledge of charge transport through these materials has the potential to hasten adoption of MOFs in energy applications.

ASSOCIATED CONTENT

Supporting Information

The Supporting Information is available free of charge at https://pubs.acs.org/doi/10.1021/acsaem.3c02456.

https://doi.org/10.1021/acsaem.3c02456
ACS Appl. Energy Mater. XXXX, XXX, XXX–XXX

Sections §1−4: (i) details of MOF precursor and MOF crystal synthesis, (ii) details of device fabrication and measurement, and (iii) details of physical characterization techniques (e.g., SEM and AFM). Figures S1−S10: (i) optical and SEM images of MOF crystals and devices, (ii) data identifying role of resist, metal evaporation, and lift-off conditions on device quality, (iii) AFM of devices, and (iv) single crystal structure of CVD grown MOF (PDF)

AUTHOR INFORMATION

Corresponding Author

Thomas J. Kempa − *Department of Chemistry and Department of Materials Science and Engineering, Johns Hopkins University, Baltimore, Maryland 21218, United States;* orcid.org/0000-0002-1672-8325; Email: tkempa@jhu.edu

Authors

Dara E. Weiss − *Department of Chemistry, Johns Hopkins University, Baltimore, Maryland 21218, United States*

Yifei Zhu − *Department of Chemistry, Johns Hopkins University, Baltimore, Maryland 21218, United States*

Kathryn Kingsbury − *Department of Chemistry, Johns Hopkins University, Baltimore, Maryland 21218, United States*

Nicholas Blumenschein − *Laboratory for Physical Sciences, College Park, Maryland 20740, United States;* orcid.org/0000-0002-6315-5734

Adam L. Friedman − *Laboratory for Physical Sciences, College Park, Maryland 20740, United States*

Aubrey T. Hanbicki − *Laboratory for Physical Sciences, College Park, Maryland 20740, United States;* orcid.org/0000-0001-8200-0378

Complete contact information is available at: https://pubs.acs.org/10.1021/acsaem.3c02456

Author Contributions

D.E.W. and T.J.K. conceived the study and designed all experiments. D.E.W. synthesized all MOFs, fabricated all devices, and collected electronic transport data with input and supervision from T.J.K. Assistance with AFM. and MOF precursor synthesis was provided by Y.Z. and K.K. Electron-beam lithography was performed at the Laboratory for Physical Sciences with input from N.B., A.L.F., and A.T.H. D.E.W. and T.J.K. wrote the manuscript.

Funding

T.J.K. acknowledges funding from a National Science Foundation (DMR-1848046) CAREER grant which supported characterization studies in this work. T.J.K. also acknowledges funding for this study by the Young Faculty Award program of the Defense Advanced Research Projects Agency (DARPA) and by the Army Research Office under Grant W911NF-21-1-0351. The views, opinions, and/or findings expressed are those of the authors and should not be interpreted as representing the official views or policies of the Department of Defense or the U.S. Government.

Notes

The authors declare no competing financial interest.

REFERENCES

(1) Hendon, C. H.; Rieth, A. J.; Korzyński, M. D.; Dincă, M. Grand Challenges and Future Opportunities for Metal-Organic Frameworks. *ACS Cent. Sci.* **2017**, *3*, 554−563.

(2) Freund, R.; Zaremba, O.; Arnauts, G.; Ameloot, R.; Skorupskii, G.; Dincă, M.; Bavykina, A.; Gascon, J.; Ejsmont, A.; Goscianska, J.; Kalmutzki, M.; Lächelt, U.; Ploetz, E.; Diercks, C. S.; Wuttke, S. The Current Status of MOF and COF Applications. *Angew. Chem., Int. Ed.* **2021**, *60*, 23975−24001.

(3) Ahmad, B. I. Z.; Keasler, K. T.; Stacy, E. E.; Meng, S.; Hicks, T. J.; Milner, P. J. MOFganic Chemistry: Challenges and Opportunities for Metal−Organic Frameworks in Synthetic Organic Chemistry. *Chem. Mater.* **2023**, *35*, 4883−4896.

(4) Ross, R. D.; Sheng, H.; Ding, Y.; Janes, A. N.; Feng, D.; Schmidt, J. R.; Segre, C. U.; Jin, S. Operando Elucidation of Electrocatalytic and Redox Mechanisms on a 2D Metal Organic Framework Catalyst for Efficient Electrosynthesis of Hydrogen Peroxide in Neutral Media. *J. Am. Chem. Soc.* **2022**, *144*, 15845−15854.

(5) Stavila, V.; Talin, A. A.; Allendorf, M. D. MOF-Based Electronic and Opto-Electronic Devices. *Chem. Soc. Rev.* **2014**, *43*, 5994−6010.

(6) Shrivastav, V.; Mansi; Gupta, B.; Dubey, P.; Deep, A.; Nogala, W.; Shrivastav, V.; Sundriyal, S. Recent Advances on Surface Mounted Metal-Organic Frameworks for Energy Storage and Conversion Applications: Trends, Challenges, and Opportunities. *Adv. Colloid Interface Sci.* **2023**, *318*, 102967.

(7) Wang, C.; Wang, C.; Xia, B.; Zhang, H.; Matavž, A.; Wang, Y.; Quan, A.; Wang, L.; Arnauts, G.; Tu, M.; Ameloot, R.; Kraft, M. A Zeolitic Imidazolate Framework-8-Coated Coupled Resonant Gas Sensor. *J. Microelectromech. Systems* **2023**, *32*, 371−380.

(8) Shekhah, O.; Liu, J.; Fischer, R. A.; Woll, C. MOF Thin Films: Existing and Future Applications. *Chem. Soc. Rev.* **2011**, *40*, 1081−1106.

(9) Gupta, R.; Jash, P.; Mondal, P. C. Nanoscale Molecular Layers for Memory Devices: Challenges and Opportunities for Commercialization. *J. Mater. Chem. C* **2021**, *9*, 11497−11516.

(10) Oh, J.; Yoon, S. M. Resistive Memory Devices Based on Reticular Materials for Electrical Information Storage. *ACS Appl. Mater. Interfaces* **2021**, *13*, 56777−56792.

(11) Kulachenkov, N.; Haar, Q.; Shipilovskikh, S.; Yankin, A.; Pierson, J.-F.; Nomine, A.; Milichko, V. A. MOF-Based Sustainable Memory Devices. *Adv. Funct. Mater.* **2022**, *32*, 2107949.

(12) Solomos, M. A.; Claire, F. J.; Kempa, T. J. 2D Molecular Crystal Lattices: Advances in their Synthesis, Characterization, and Application. *J. Mater. Chem. A* **2019**, *7*, 23537−23562.

(13) Claire, F. J.; Solomos, M. A.; Kim, J.; Wang, G.; Siegler, M. A.; Crommie, M. F.; Kempa, T. J. Structural and Electronic Switching of a Single Crystal 2D Metal-Organic Framework Prepared by Chemical Vapor Deposition. *Nature Commun.* **2020**, *11* (5524), 1−8.

(14) Li, M. M.; Claire, F. J.; Solomos, M. A.; Tenney, S. M.; Ivanov, S. A.; Siegler, M. A.; Kempa, T. J. Molecular Chains of Coordinated Dimolybdenum Isonicotinate Paddlewheel Clusters. *RSC Adv.* **2019**, *9*, 16492−16495.

(15) Day, R. W.; Bediako, D. K.; Rezaee, M.; Parent, L. R.; Skorupskii, G.; Arguilla, M. Q.; Hendon, C. H.; Stassen, I.; Gianneschi, N. C.; Kim, P.; Dincă, M. Single Crystals of Electrically Conductive Two-Dimensional Metal-Organic Frameworks: Structural and Electrical Transport Properties. *ACS Cent. Sci.* **2019**, *5*, 1959−1964.

(16) Waser, R. *Nanoelectronics and Information Technology Advanced Electronic Materials and Novel Devices*, 2nd ed.; John Wiley and Sons, Inc., 2005.

(17) Stassen, I.; Burtch, N.; Talin, A.; Falcaro, P.; Allendorf, M.; Ameloot, R. An Updated Roadmap for the Integration of Metal-Organic Frameworks with Electronic Devices and Chemical Sensors. *Chem. Soc. Rev.* **2017**, *46*, 3185−3241.

(18) Pomerantseva, E.; Bonaccorso, F.; Feng, X.; Cui, Y.; Gogotsi, Y. Energy Storage: The Future Enabled by Nanomaterials. *Science* **2019**, *366*, No. eaan8285. 1−12.

(19) Hanna, S. L.; Barsoum, M.; Debela, T. T.; Malliakas, C. D.; Gaidimas, M. A.; Knapp, J. G.; Kirlikovali, K. O.; Hendon, C. H.; Dravid, V. P.; Farha, O. K. Mapping the Complete Reaction Energy Landscape of a Metal−Organic Framework Phase Transformation. *ACS Mater. Lett.* **2023**, *5*, 2518−2527.
(20) Kurandina, D.; Huang, B.; Xu, W.; Hanikel, N.; Darù, A.; Stroscio, G. D.; Wang, K.; Gagliardi, L.; Toste, F. D.; Yaghi, O. M. A Porous Crystalline Nitrone-Linked Covalent Organic Framework. *Angew. Chem., Int. Ed.* **2023**, *135*, No. e202307674. 1−5.
(21) Uliana, A. A.; Bui, N. T.; Kamcev, J.; Taylor, M. K.; Urban, J. J.; Long, J. R. Ion-Capture Electrodialysis Using Multifunctional Adsorptive Membranes. *Science* **2021**, *372*, 296−299.
(22) Evans, A. M.; Parent, L. R.; Flanders, N. C.; Bisbey, R. P.; Vitaku, E.; Kirschner, M. S.; Schaller, R. D.; Chen, L. X.; Gianneschi, N. C.; Dichtel, W. R. Seeded Growth of Single-Crystal Two-Dimensional Covalent Organic Frameworks. *Science* **2018**, *361*, 52−57.
(23) Sze, S.M.; Lee, M. K.. *Semiconductor Devices: Physics and Technology Third ed.*, 3rd ed.; John Wiley and Sons, Inc., 2012.
(24) Ko, M.; Mendecki, L.; Mirica, K. A. Conductive Two-Dimensional Metal-Organic Frameworks as Multifunctional Materials. *Chem. Commun.* **2018**, *54*, 7873−7891.
(25) Campbell, M. G.; Dincă, M. Metal-Organic Frameworks as Active Materials in Electronic Sensor Devices. *Sensors* **2017**, *17*, 1108.
(26) Allendorf, M. D.; Dong, R.; Feng, X.; Kaskel, S.; Matoga, D.; Stavila, V. Electronic Devices Using Open Framework Materials. *Chem. Rev.* **2020**, *120*, 8581−8640.
(27) Sato, O. Dynamic Molecular Crystals with Switchable Physical Properties. *Nat. Chem.* **2016**, *8*, 644−656.
(28) Ziebel, M. E.; Darago, L. E.; Long, J. R. Control of Electronic Structure and Conductivity in Two-Dimensional Metal-Semiquinoid Frameworks of Titanium, Vanadium, and Chromium. *J. Am. Chem. Soc.* **2018**, *140*, 3040−3051.
(29) Xie, L. S.; Sun, L.; Wan, R.; Park, S. S.; DeGayner, J. A.; Hendon, C. H.; Dincă, M. Tunable Mixed-Valence Doping toward Record Electrical Conductivity in a Three-Dimensional Metal-Organic Framework. *J. Am. Chem. Soc.* **2018**, *140*, 7411−7414.
(30) Park, J. G.; Aubrey, M. L.; Oktawiec, J.; Chakarawet, K.; Darago, L. E.; Grandjean, F.; Long, G. J.; Long, J. R. Charge Delocalization and Bulk Electronic Conductivity in the Mixed-Valence Metal-Organic Framework Fe(1,2,3-Triazolate)$_2$(BF_4)$_x$. *J. Am. Chem. Soc.* **2018**, *140*, 8526−8534.
(31) Kempa, T. J.; Tian, B.; Kim, D. R.; Hu, J.; Zheng, X.; Lieber, C. M. Single and Tandem Axial p-i-n Nanowire Photovoltaic Devices. *Nano Lett.* **2008**, *8*, 3456−3460.
(32) Kempa, T. J.; Lieber, C. M. Semiconductor Nanowire Solar Cells: Synthetic Advances and Tunable Properties. *Pure Appl. Chem.* **2014**, *86*, 13−26.
(33) Carter, C. B.; Williams, D. B. *Transmission Electron Microscopy: A Textbook for Materials Science*; 2nd ed.; Springer, 2009.
(34) Egerton, R. F.; Li, P.; Malac, M. Radiation Damage in the TEM and SEM. *Micron.* **2004**, *35*, 399−409.
(35) Gu, H.; Li, G.; Liu, C.; Yuan, F.; Han, F.; Zhang, L.; Wu, S. Considerable Knock-on Displacement of Metal Atoms under a Low Energy Electron Beam. *Sci. Rep.* **2017**, *7* (180), 1−10.
(36) Yumusak, G.; Leyland, A.; Matthews, A. The Effect of Pre-Deposited Titanium-Based PVD Metallic Thin Films on the Nitrogen Diffusion Efficiency and Wear Behaviour of Nitrided Ti Alloys. *Surf. Coat. Technol.* **2020**, *394*, 125545.
(37) Cotton, F. A.; Dalal, N. S.; Liu, C. Y.; Murillo, C. A.; North, J. M.; Wang, X. Fully localized mixed-valence oxidation products of molecules containing two linked dimolybdenum units: An effective structural criterion. *J. Am. Chem. Soc.* **2003**, *125*, 12945−12952.
(38) Andersen, C. E.; McPherson, J. N.; Gimenez-Marques, M.; Li, J.; Kubus, M.; Ito, S.; Gob, C. R.; Ott, S.; Larsen, R. W.; Minguez Espallargas, G.; Pedersen, K. S. Vapor-phase synthesis of low-valent metal-organic frameworks from metal carbonyl synthons. *J. Mater. Chem. C* **2023**, *11*, 11460.
(39) Squire, I. A. Z.; Goult, C. A.; Thompson, B. C.; Alexopoulos, E.; Whitwood, A. C.; Tanner, T. F. N.; Wilkinson, L. A. Enhancing the air stability of dimolybdenum paddlewheel complexes: Redox tuning through fluorine substituents. *Inorg. Chem.* **2022**, *61*, 19144−19155.
(40) Chakraborty, A.; Ilic, S.; Cai, M.; Gibbons, B. J.; Yang, X.; Slamowitz, C. C.; Morris, A. J. Role of spin-orbit coupling in long range energy transfer in metal-organic frameworks. *J. Am. Chem. Soc.* **2020**, *142*, 20434−20443.

https://doi.org/10.1021/acsaem.3c02456
ACS Appl. Energy Mater. XXXX, XXX, XXX−XXX